

# Effects of types of bridge decks on competitive relationships between aerostatic and flutter stability for a super long cable-stayed bridge

Chuanxin Hu<sup>a</sup>, Zhiyong Zhou<sup>\*</sup> and Baosong Jiang<sup>b</sup>

State Key Laboratory of Disaster Reduction in Civil Engineering, Tongji University, Shanghai, No. 1239, Siping Road, China

(Received February 27, 2018, Revised November 3, 2018, Accepted February 5, 2019)

**Abstract.** Aerodynamic configurations of bridge decks have significant effects on the aerostatic torsional divergence and flutter for super long-span bridges, which are onset for selection of suitable bridge decks for those bridges. Based on a cable-stayed bridge with double main spans of 1500 m, considering typical twin-box, stiffening truss and closed-box section, which are the most commonly used form of bridge decks and assumed that the rigidity of those section is completely equivalent, are utilized to investigate the effects of aerodynamic configurations of bridge decks on aerodynamic instability performance comprised of the aerostatic torsional divergence and flutter, by means of wind tunnel tests and numerical calculations, including three-dimensional (3D) multimode flutter analysis and nonlinear aerostatic analysis. Regarding the aerostatic torsional divergence, the results obtained in this study show twin-box section is the best, closed-box section the second-best, and the stiffening truss section the worst. Regarding the flutter, the flutter stability of the twin-box section is far better than that of the stiffening truss and closed-box section. Furthermore, wind-resistance design depends on the torsional divergence for the twin-box and stiffening truss section. However, there are obvious competitive relationships between the aerostatic torsional divergence and flutter for the closed-box section. Flutter occur before aerostatic instability at initial attack angle of  $+3^\circ$  and  $0^\circ$ , while the aerostatic torsional divergence occur before flutter at initial attack angle of  $-3^\circ$ . The twin-box section is the best in terms of both aerostatic and flutter stability among those bridge decks. Then mechanisms of aerostatic torsional divergence are revealed by tracking the cable forces synchronous with deformation of the bridge decks in the instability process. It was also found that the onset wind velocities of these bridge decks are very similar at attack angle of  $-3^\circ$ . This indicates that a stable triangular structure made up of the cable planes, the tower, and the bridge deck greatly improves the aerostatic stability of the structure, while the aerodynamic effects associated with the aerodynamic configurations of the bridge decks have little effects on the aerostatic stability at initial attack angle of  $-3^\circ$ . In addition, instability patterns of the bridge depend on both the initial attack angles and aerodynamic configurations of the bridge decks. This study is helpful in determining bridge decks for super long-span bridges in future.

**Keywords:** cable-stayed bridge; aerodynamic configurations; wind-induced stability; flutter; aerostatic torsional divergence

## 1. Introduction

In recent decades, cable-supported bridges, involving cable-stayed and suspension bridges, have been the most popular types of bridges. Longer and longer spans are being planned, such as the Xihoumen suspension bridge in China with a central span of 1650 m (Yang *et al.* 2007), the Messina Bridge in Italy (Diana *et al.* 2004), a suspension bridge expected to stretch 3300 m, and the Qiongzhou strait Bridge in China, a cable-stayed bridge with double main spans of 1500 m. Greater attention has been placed on the aerodynamic performance of ultra-thousand long-span bridges which are sensitive to wind excitations. Both aerostatic torsional divergence and flutter are challenging for the wind-resistant performance of long-span cable-

stayed bridges.

Considerable attention has been drawn to the flutter performance of long-span bridges (e.g., Kusano *et al.* 2014, Mannini *et al.* 2015, Argentini *et al.* 2016), and aerodynamic configurations of bridge decks are one of the most important factors affecting this performance. Closed-box, twin-box, and stiffening

truss sections have been comprehensively used as bridge decks for super long-span bridges, especially ultra-thousand-meter span bridges. Previous research has shown that streamlined closed-box sections are one of the most competitive bridge decks due to their high flutter performance. The Sutong Yangtze River Bridge with a main span of 1088 m, and the Taizhou Bridge with double main spans of 1080 m each, are considered good examples of the application of this type of bridge decks. However, as the spans increase, the closed-box sections cease to meet the requirements of flutter stability. This is an effective aerodynamic measure that can improve the onset wind velocity of flutter by slotting in the closed-box section, also called multi-box section. It has been demonstrated that a twin-box section has better flutter stability than a closed-box section (Ge and Xiang 2009). To date, several super-long-span bridges have been built with this type of bridge

\*Corresponding author, Professor

E-mail: Z.zhou@tongji.edu.cn

<sup>a</sup> Ph.D. Student

E-mail: chuanxinhoo@tongji.edu.cn

<sup>b</sup> Ph.D. Student

E-mail: jbs0645@163.com

deck, including the Xihoumen Bridge in China, which has a main span of 1650 m (Yang *et al.* 2007); the Yi Sun-sin Bridge in Korea, which has a main span of 1545 m (Laima *et al.* 2015); and Messina Strait Bridge in Italy, which has a main span of 3300 m and a triple-box section (Diana *et al.* 1995). The understanding of aerostatic torsional divergence and flutter of multi-box sections has been significantly improved over the last several decades (e.g., Lee *et al.* 2014, Yang *et al.* 2015, Trein *et al.* 2015, Miranda *et al.* 2015). Due to limited construction conditions in mountainous areas in China and good flutter performance, stiffening truss sections are usually one of the best choices for long-span bridges, which are adopted by the Akashi Kaikyo Bridge in Japan with a main span of 1991 m (Kitagawa *et al.* 2004) and the Dongtinghu second Bridge with a main span of 1480 m in China. However, despite the efforts made in the past, there have been few comparative studies of the flutter performance of closed-box, twin-box, and stiffening truss sections, which are onset for selection of suitable bridge decks for super-long-span bridges for structural and wind engineers.

Theoretical methods for aerostatic instability analysis have gradually been improved, and the methods of analyzing the three-dimensional nonlinear aerostatic stability of long-span bridges have been used comprehensively. Among these methods, the most typical is the incremental-two-iterative method, proposed by Cheng (2002, 2003). The effects of bridge spans on the aerostatic and flutter stability were investigated (Chen *et al.* 2000). A series of parameter sensitivity analysis on aerostatic stability have been studied (Zhang *et al.* 2007; Li *et al.* 2014). Results showed that aerodynamic configurations are one of the most important factors affecting the aerostatic stability of bridges (Cheng *et al.* 2001). Zhang *et al.* (2013) investigated the mechanism of the aerostatic torsional divergence of long-span suspension bridges on the basis of a generalized model. The outcome showed that the vertical motion of a bridge deck was crucial to the torsional stiffness of the whole suspended system, and that the vertical motion of either cable with a magnitude beyond a certain threshold could result in a sudden degradation of the torsional stiffness of the system. Most current research has been performed on bridge engineering projects, and the analysis of aerostatic stability and flutter stability were conducted separately, disregarding the relationships between them, which can differ for different aerodynamic configurations. In the past, it was generally believed that the onset wind velocities of flutter were generally lower than those of aerostatic instability for super long-span bridges. However, recent research has shown there to be competitive relationships between aerostatic instability and flutter that increase in intensity as the span increases for super long-span bridges, and aerostatic instability may occur before flutter. Lateral-torsional buckling was first observed in a suspension bridge under the action of static wind loads in wind tunnel tests of the full bridge model (Hirai *et al.* 1967). It was later observed in cable-stayed bridges in the wind tunnel laboratory of Tongji University (Ge *et al.* 2011). Boonyapinyo *et al.* (1994, 2006) performed numerical examples on the aerostatic instability and flutter of the

Akashi Kaikyo Bridge with a main span length of 1990 m. The results indicated that the onset wind velocity of nonlinear aerostatic instability was significantly lower than the onset wind velocity of flutter.

In conclusion, the aerodynamic configurations of the bridge decks are an important factor affecting both aerostatic and flutter stability of long-span bridges. However, the effects of the aerodynamic configurations on competitive relationships between them have not been reported yet. In view of how widely used sections are in long-span bridges, a typical twin-box, stiffening truss, and closed-box section are chosen as typical aerodynamic configurations to investigate the effects of aerodynamic configurations on aerostatic instability and flutter instability and the relationships between them by means of combination of wind tunnel tests and numerical calculations, based on a cable-stayed bridge with double spans of 1500 m.

This study is organized as follows: Section 2 presents a super long-span cable-stayed bridge as an example for the numerical modeling, and typical sections, involving twin-box, stiffening truss, and closed-box section, are also introduced. Besides, related aerodynamic parameters obtained from wind tunnel tests, including static aerodynamic coefficients and flutter derivatives, are also illustrated in this section. Section 3 illustrates the nonlinear aerostatic analysis method as well as related key parameters in this study for the determination of onset wind velocity of aerostatic instability. Section 4 presents the discussion on the results obtained, especially the competitive relationships between aerostatic torsional divergence and flutter. Thereafter, mechanism of aerostatic torsional divergence are revealed in Section 5. Finally, future prospects and conclusions of the current study are briefly expressed in Section 6.

## 2. Numerical example

A super long-span cable-stayed bridge is utilized to investigate effects of aerodynamic configurations on aerostatic torsional divergence, flutter, and the competitive relationships between them, assumed that the rigidity of the bridge decks under different aerodynamic configurations is completely equivalent, since the main purpose of this paper is to study the effects of aerodynamic configurations on the aerostatic and flutter stability of long-span bridges, disregarding variations in structural stiffness attributable to different bridge decks.

### 2.1 Bridge system

A stayed-cable bridge with double main spans of 1500m and two side spans of 652 m is here investigated, as shown in Fig. 1, and a twin-box section is shown in Fig. 2, indicated by TB section in following Figures and Tables.

A three-dimensional finite element model was established using commercial software ANSYS10.0, based on the bridge system and bridge deck in Fig. 2. Three-dimensional beam elements were used to model the towers and piers. The cables were modeled using multi-segment

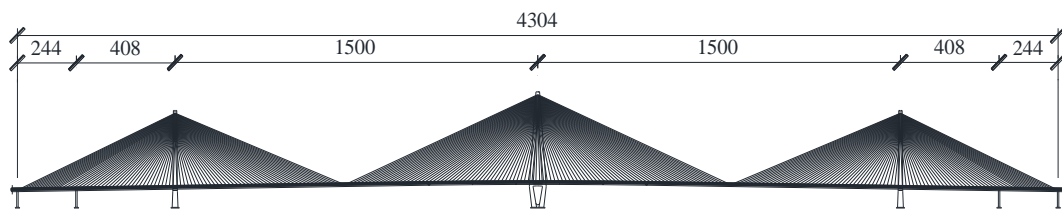


Fig. 1 General layout of a cable-stayed bridge (Unit: m)

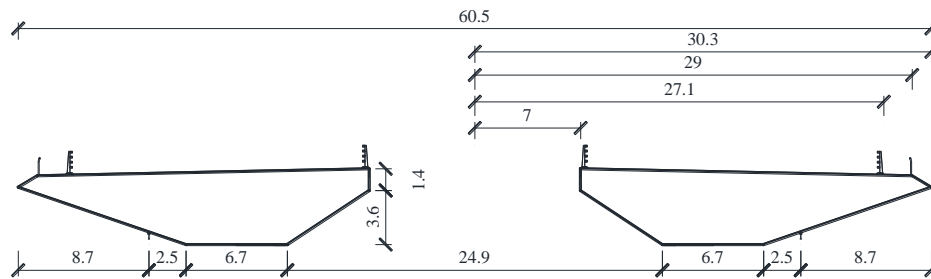
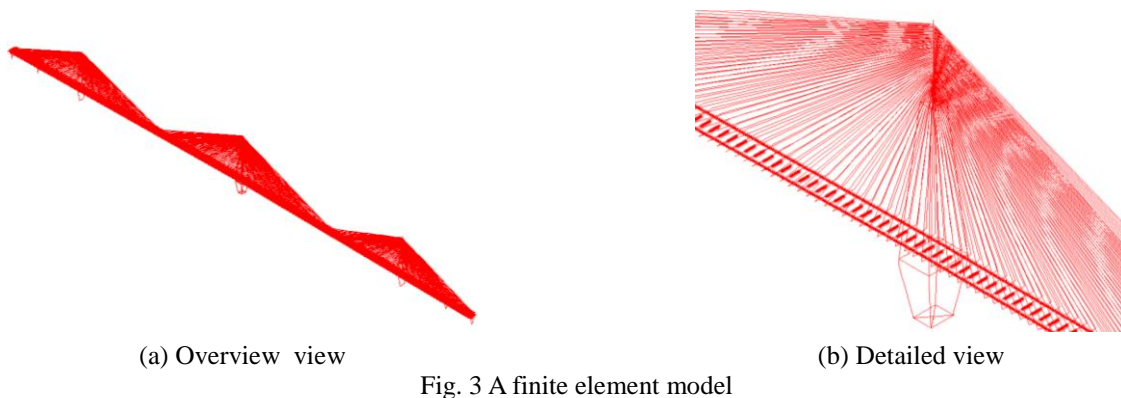


Fig. 2 Configuration of a twin-box section (Unit: m)



(a) Overview view

(b) Detailed view

Fig. 3 A finite element model

Table 1 Structural parameters of the bridge

Parameters	Values
Main span length	1500.0 m
Cable center distance	55.00 m
Cable diameter	0.083 m - 0.124 m
Deck section area(single box)	1.1199 m <sup>2</sup>
Vertical moment inertia of deck(single box)	3.2664 m <sup>4</sup>
Lateral moment inertia of deck(single box)	50.994 m <sup>4</sup>
Torsional moment inertia of deck(single box)	7.5167 m <sup>4</sup>
Deck mass per unit length(single box)	17018.0 kg/m
Deck mass moment per unit length(single box)	715877.7 kg·m <sup>2</sup> /m

three-dimensional truss elements, accounting for geometric nonlinearity due to cable sag. The double-girder model proposed by Zhu *et al.* (2000) was used to model the bridge deck, and the sectional properties of the bridge deck were

assigned to the beam as equivalent properties. Structural parameters of the bridge system are listed in Fig. 1, and a finite element model is shown in Fig. 3.

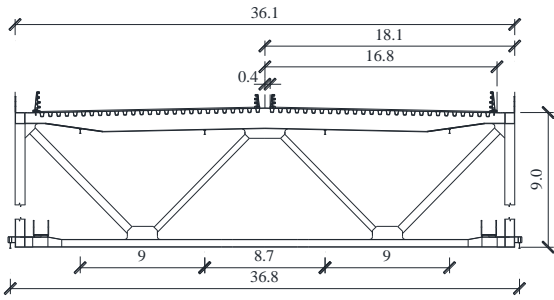


Fig. 4 Configuration of a stiffening truss section (Unit: m)

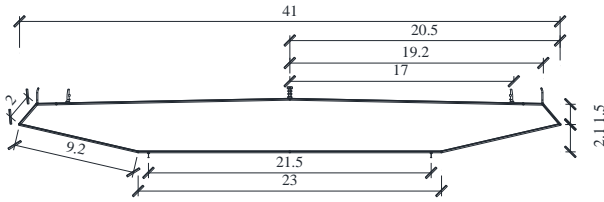


Fig. 5 Configuration of a closed-box section (Unit: m)

The stiffening truss section and closed-box section are also chosen as bridge decks in this study, indicated by ST section, and CB section respectively in following Figures and Tables, as shown in Figs. 4 and 5 respectively.

## 2.2 Aerodynamic parameters

Aerodynamic parameters in this study, involving static aerodynamic coefficients and flutter derivatives, are obtained in wind tunnels for numerical calculations in following sections. The Reynolds number in ordinary wind tunnel tests of the bridge deck has been generally  $10^2$  to  $10^3$  times smaller than that at actual bridges, so static aerodynamic coefficients and flutter derivatives of bridge decks are reported to be remarkably dependent on Reynolds number (e.g., Schewe and Larsen 1998, Schewe 2001, Matsuda *et al.* 2001, Larose and D'outeuil 2006, Li *et al.* 2014). In spite of those limitations, previous research indicate that conventional wind tunnel test results in the low Reynolds number region are conservative for wind resistant-design of bridge decks (Matsuda *et al.* 2001).

### 2.2.1 Static aerodynamic coefficients

The static aerodynamic coefficients, as shown in Fig. 6, can be written in the wind axes as follows

$$C_D(\alpha) = \frac{F_D(\alpha)}{\frac{1}{2}\rho U^2 H} \quad (1a)$$

$$C_L(\alpha) = \frac{F_L(\alpha)}{\frac{1}{2}\rho U^2 B} \quad (1b)$$

$$C_M(\alpha) = \frac{M_z(\alpha)}{\frac{1}{2}\rho U^2 B^2} \quad (1c)$$

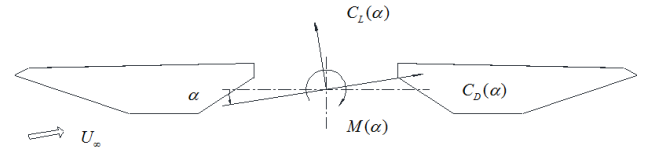


Fig. 6 Schematic diagram of static aerodynamic coefficients

In Eq. (1),  $C_D(\alpha)$ ,  $C_L(\alpha)$ , and  $C_M(\alpha)$  are the static aerodynamic coefficients in the wind axes;  $F_D(\alpha)$ ,  $F_L(\alpha)$ , and  $F_M(\alpha)$  are the drag, lift, and pitching moment in the wind axes, respectively, representing the three-component displacement-dependent wind loads per unit span acting on the deformed bridge deck;  $U$  is the mean wind velocity;  $\rho$  is the air density;  $B$  is the deck width, 60.5 m, 36.1 m and 41.0 m for twin-box section, stiffening truss section and closed-box section respectively;  $H$  is the deck height, 5.0 m, 9.0 m and 3.6 m for twin-box section, stiffening truss section and closed-box section respectively; and  $\alpha$  is the wind angle of attack. As shown in Fig. 6, if the wind attack angle  $\alpha$  is zero, the wind axes coincide with the bridge axes.

The drag, lift, and pitching moment coefficients for the twin-box section, stiffening truss section and closed-box section were measured in wind tunnel. Geometrical scales of the sectional models for these bridge decks are 1:80, 1:70 and 1:70 respectively, and test velocity are 10m/s, 10 m/s, and 12 m/s respectively, with corresponding Reynolds numbers of  $5.11 \times 10^5$ ,  $3.48 \times 10^5$ , and  $3.96 \times 10^5$  respectively. The Reynolds number are defined as the ratio of the fluid inertia force to the fluid viscous force  $Re = UH/\nu$ . where  $\nu$  is the kinematic viscosity.

The comparison of drag, lift and pitching moment coefficients between different bridge decks are shown in Figs. 7(a)-7(c), respectively. The aerostatic instability of bridges is closely related to characteristics of these coefficients, and the onset wind velocities of aerostatic instability are inversely proportional to the slopes of the pitching moment (Chen *et al.* 2001). Fig. 7(d) also illustrates the slope of pitching moment as a function of attack angle for different bridge decks.

Drag coefficients of the twin-box section are larger than those of the stiffening truss section and the closed-box section in all attack angles listed, while the lift coefficients of the stiffening truss section are larger than those of the twin-box section and closed-box section. The absolute values of pitching moment coefficients of the stiffening truss section are greater than those of the twin-box section and closed-box section at high attack angles. Lift coefficients of the stiffening truss section and closed-box section change abruptly at attack angle of  $+10^\circ$  and  $+5^\circ$ , respectively, with variations in the attack angle, and then the slopes of the lift coefficients rapidly approach zero. Slopes of the pitching moment coefficients for the closed-box section decrease with attack angle in the range of the positive attack angles, while those for the stiffening truss section decline sharply after attack angle of  $+7^\circ$ . In addition, slopes of the pitching moment coefficients for the twin-box

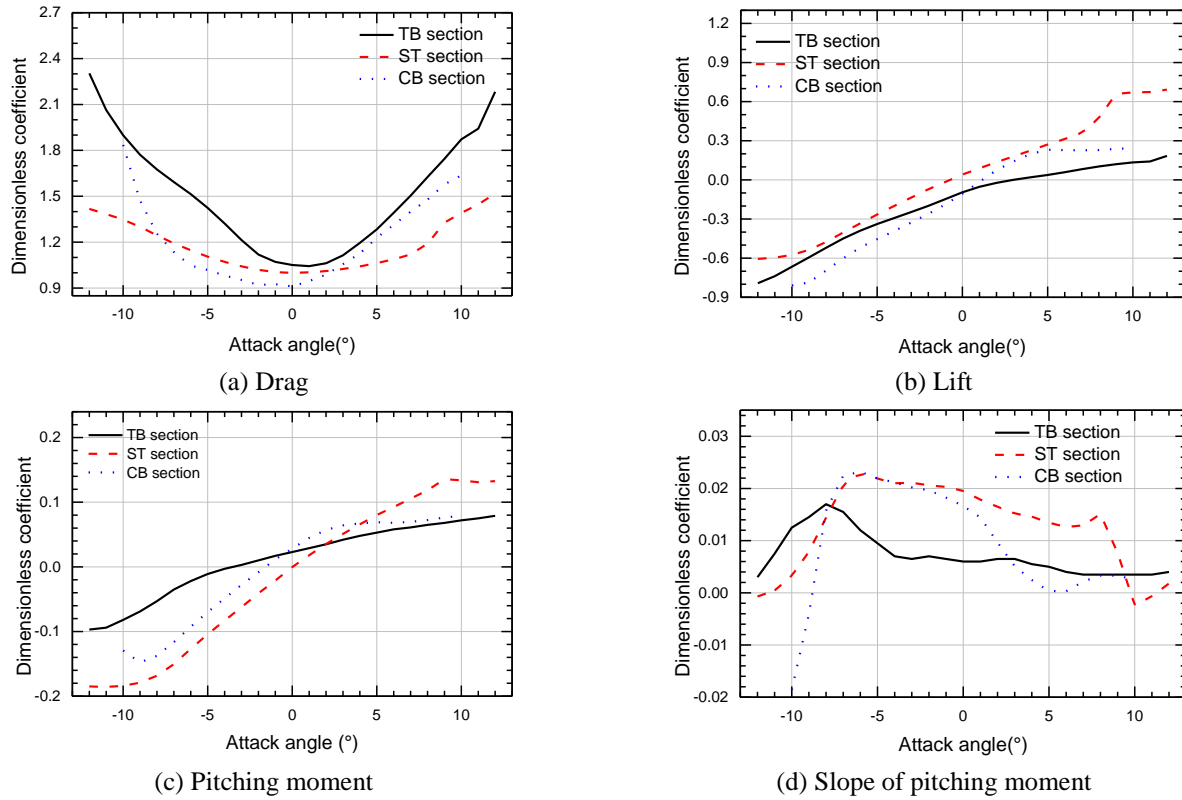


Fig. 7 Comparison of static aerodynamic coefficients between different bridge decks

section vary slightly with the attack angle, compared with the other sections.

### 2.2.2 Flutter derivatives

The self-excited forces for bridge decks are most commonly represented by flutter derivatives, as suggested by Scanlan (1978, 1993). Unsteady self-excited aerodynamic forces per unit span in extended format for a section can be expressed as follows

$$L_{se} = \frac{1}{2} \rho U^2 (2B) \left[ KH_1^* \frac{\dot{h}}{U} + KH_2^* \frac{B\dot{\alpha}}{U} + K^2 H_3^* \alpha + K^2 H_4^* \frac{h}{B} + KH_5^* \frac{\dot{p}}{B} + K^2 H_6^* \frac{p}{B} \right] \quad (2a)$$

$$D_{se} = \frac{1}{2} \rho U^2 (2B) \left[ KP_1^* \frac{\dot{p}}{U} + KP_2^* \frac{B\dot{\alpha}}{U} + K^2 P_3^* \alpha + K^2 P_4^* \frac{p}{B} + KA_5^* \frac{\dot{h}}{B} + K^2 A_6^* \frac{h}{B} \right] \quad (2b)$$

$$M_{se} = \frac{1}{2} \rho U^2 (2B^2) \left[ KA_1^* \frac{\dot{h}}{U} + KA_2^* \frac{B\dot{\alpha}}{U} + K^2 A_3^* \alpha + K^2 A_4^* \frac{h}{B} + KA_5^* \frac{\dot{p}}{B} + K^2 A_6^* \frac{p}{B} \right] \quad (2c)$$

Here,  $\rho$  is the air density;  $\omega$  represents the circular frequencies;  $K = \omega B / U$  is the reduced frequency.  $h$ ,  $\alpha$  and  $p$  are the vertical, torsional and lateral displacements, respectively;  $\dot{h}$ ,  $\dot{\alpha}$  and  $\dot{p}$  are the vertical, torsional and lateral velocity, respectively. The over dot denotes the partial differentiation with respect to time  $t$ ;  $H_i^*$ ,  $A_i^*$  and  $P_i^*$  ( $i=1,2,3,4,5,6$ ) are the dimensionless flutter derivatives, which are assumed to be sectional properties as functions of the reduced frequency.

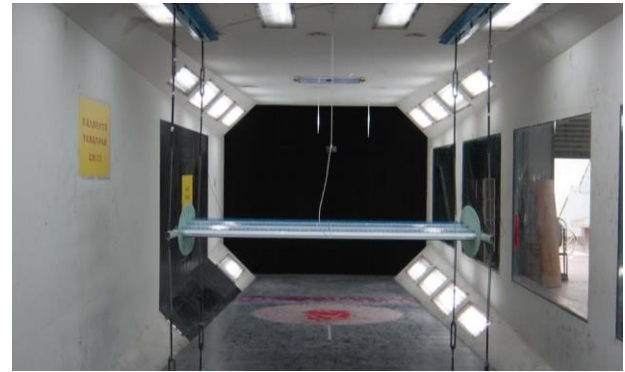
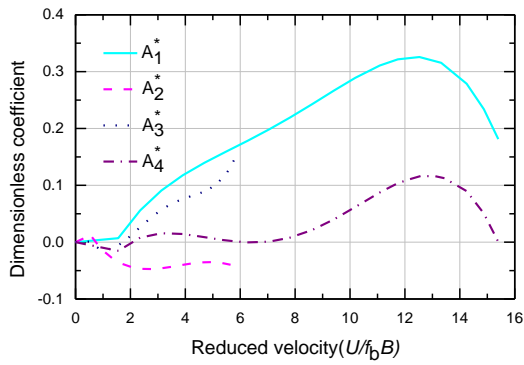


Fig. 8 Experimental setup in TJ-2 wind tunnel

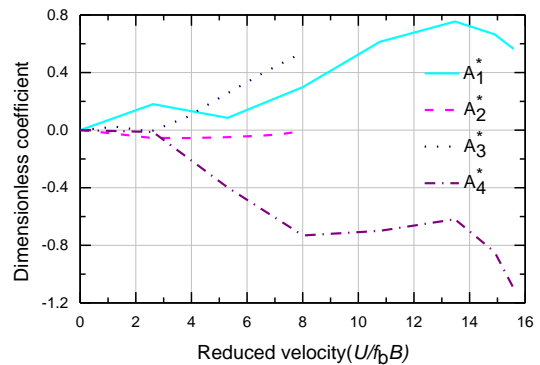
Based on the free vibration tests of a spring-suspended sectional model (SSSM), the modified least-square method in time domain proposed by Ding *et al.* (2002) was used to identify the flutter derivatives related to vertical and torsional motions, i.e.,  $H_i^*$  and  $A_i^*$  ( $i=1,2,3,4$ ). A stepped factor is proposed in this method to avoid the divergence caused by noise in solving the nonlinear parameters through iterations. The SSSM was installed on the frame-supported system in TJ-2 wind tunnel, with thin elliptical end-plates attached to each side of the sectional model and two laser displacement sensors at each end, as shown in Fig. 8. The parameters of the sectional models are listed in Table 2. MLS LM10-130 ANR1215-type laser displacement transducers are used for displacement

Table 2 Parameters of the sectional models

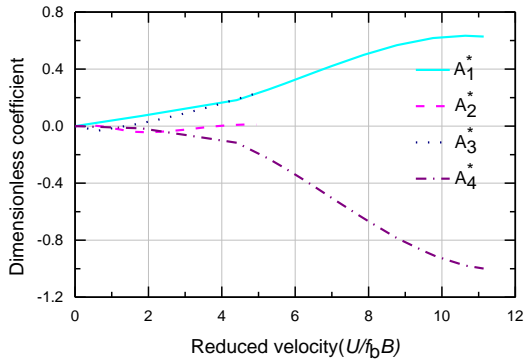
		Properties Geometric	TB section	ST section	CB section
Geometric scale	Scale ratio		1: 80	1: 70	1: 70
	Width ( $B$ /m)		0.756	0.516	0.586
	Height ( $H$ /m)		0.063	0.129	0.051
Equivalent mass	Mass/unit length ( $m$ /kg/m)		8.495	8.0982	6.53
	Mass moment of inertia/unit length ( $I_m$ /kg.m <sup>2</sup> /m)		0.383	0.3054	0.379
Frequency	Vertical ( $f_b$ /Hz)		3.294	1.465	1.965
	Torsional ( $f_t$ /Hz)		9.397	3.070	5.786
Damping ratio	Vertical ( $\xi_b$ /‰)		3.2	4.5	3.4~4.2
	Torsional ( $\xi_t$ /‰)		4.2	2.1	1.3~1.5



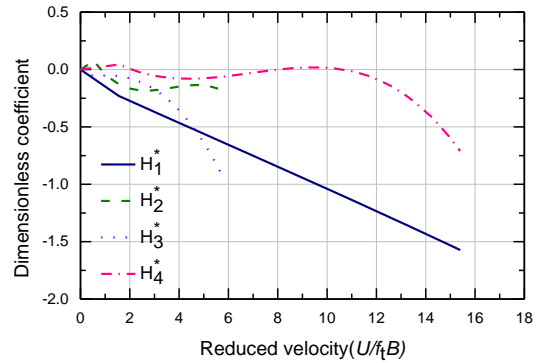
(a) TB section ( $A_1^* \sim A_4^*$ )



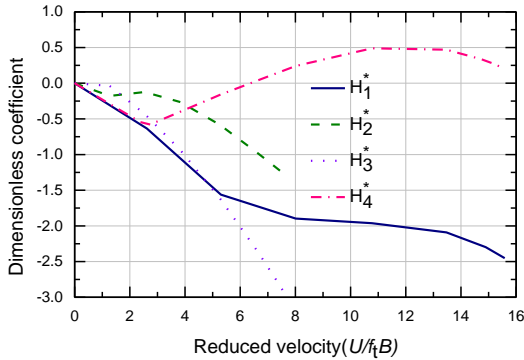
(b) ST section ( $A_1^* \sim A_4^*$ )



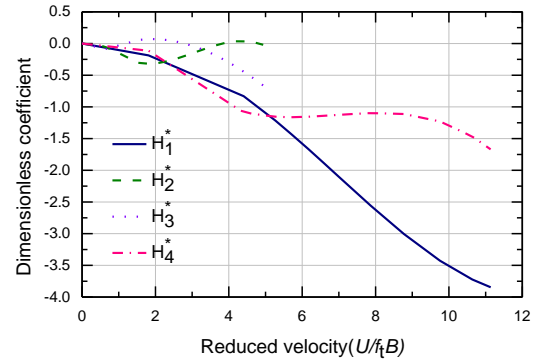
(c) CB section ( $A_1^* \sim A_4^*$ )



(d) TB section ( $H_1^* \sim H_4^*$ )

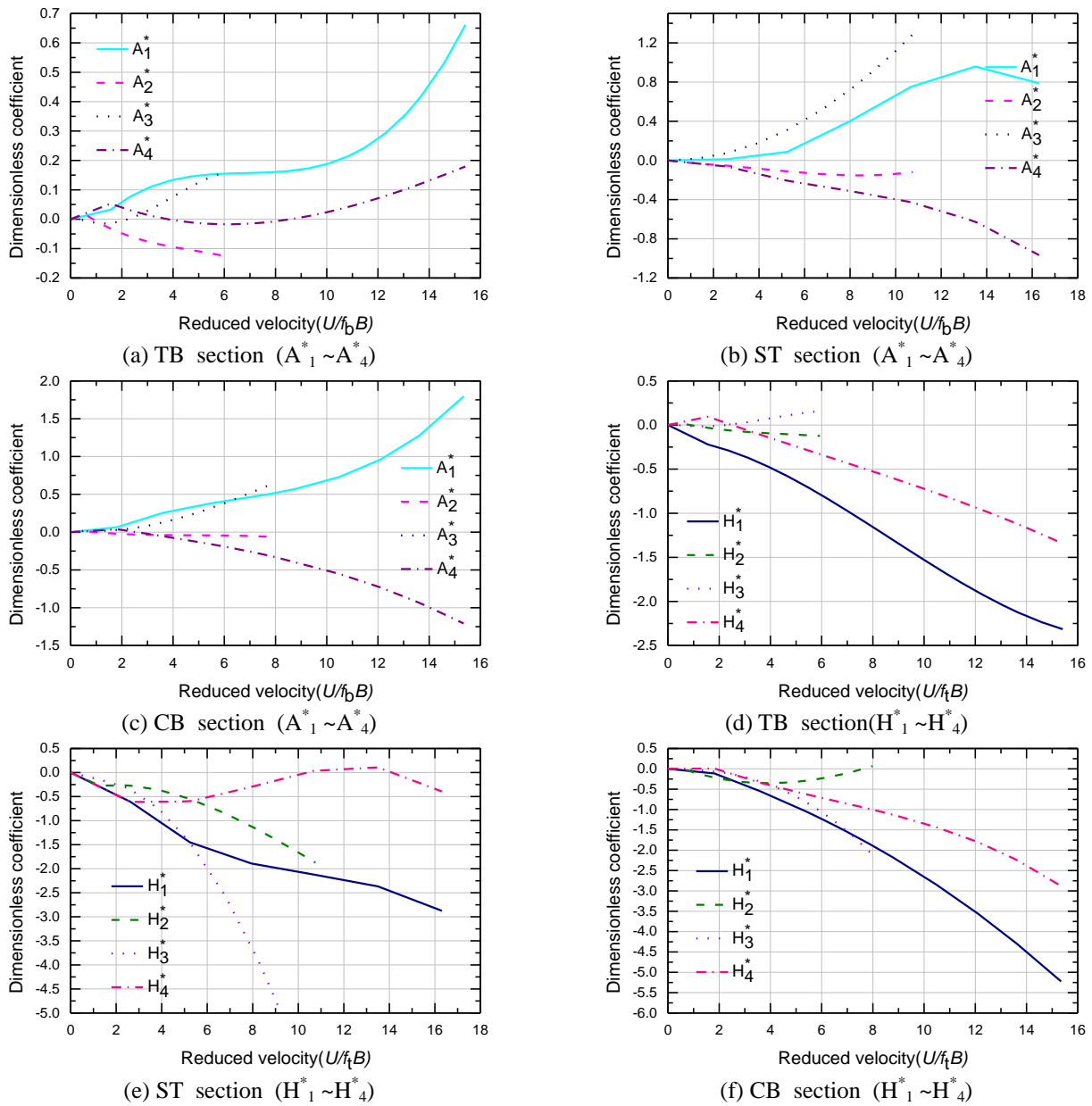


(e) ST section ( $H_1^* \sim H_4^*$ )



(f) CB section ( $H_1^* \sim H_4^*$ )

Fig. 9 Flutter derivatives at initial attack angle of  $+3^\circ$

Fig. 10 Flutter derivatives at initial attack angle of  $0^\circ$ 

measurements, with a measuring range of  $130 \pm 50$  mm, a resolution of  $20 \mu\text{m}$ , and a maximal linearity error of less than  $\pm 0.2\%$ . The maximum blocking ratio during the tests is less than 5%. Flutter derivatives for the bridge decks above related to vertical and torsional motions at initial attack angle of  $+3^\circ$ ,  $0^\circ$ , and  $-3^\circ$  are shown in Figs. 9-11 respectively.

### 3. Method of nonlinear aerostatic analysis

In order to determine the onset wind velocity of aerostatic torsional divergence, the geometric nonlinearity of structure and displacement-dependent wind loads, which

are a nonlinear function of effective wind attack angle comprised of initial attack angle and torsional component of the bridge deck due to displacement-dependent wind loads, are here considered, disregarding the effects of material nonlinearity on aerostatic instability. An incremental-two-iterative method (Chen *et al.* 2002) is used in this study to calculate the onset velocity. Besides, several key parameters need to be determined in order to precisely obtain responses of the bridge under the action of strong wind.

The length and number of cables increase as the span of the bridge increase. The wind loads acting on the cable have a pronounced influence on its deformation.

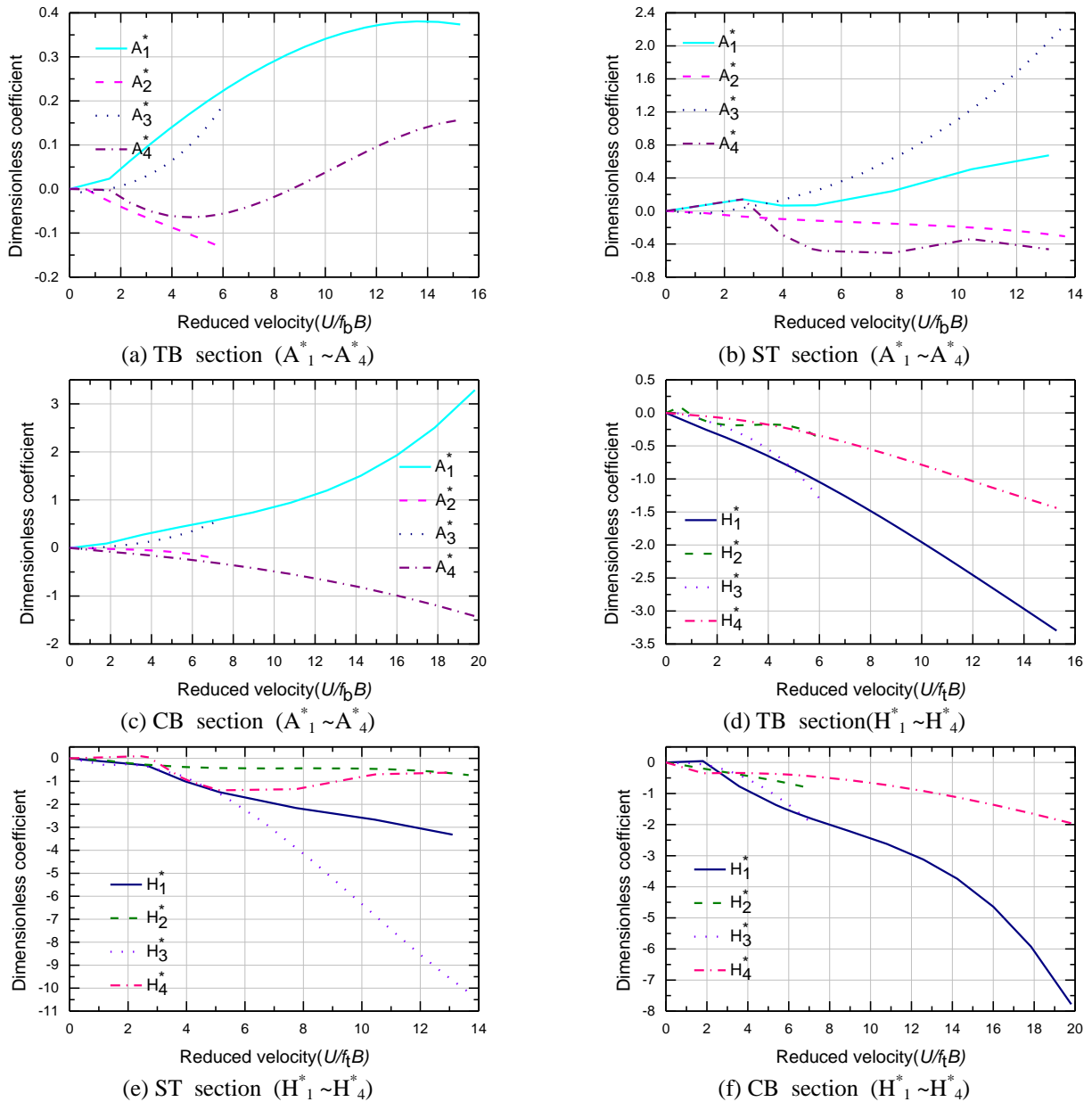


Fig. 11 Flutter derivatives at initial attack angle of  $-3^\circ$

If the wind loads on the cables are directly applied to the nodes of towers and the girders connected to the cables, the deformation caused by wind loads on the cables of the bridges and the consequent changes in the direction and size of the cable tensions cannot be indicated accurately. Then the restraints and displacements of the bridge decks cannot be modeled precisely, which can affect the overall aerostatic stability of the bridges. In this way, the multi-segmental truss element can be used to simulate the cable. Variation in the torsional and vertical displacement with divisions of a single cable were calculated at wind velocity of 110 m/s, taking the initial wind attack angle of  $0^\circ$  (twin-box section) as trial case to determine divisions of cables in nonlinear aerostatic analysis, as shown in Fig. 12(a). It should be noted that the direction of vertical and torsional

displacement is same as that of the lift and pitching moment in this paper. That is, the bridge deck moves upwards when value of vertical displacement is positive, and downwards when negative. The results indicate that the errors are very small when there are 20 or more divisions. Therefore, all cables of the bridge have been divided into 20 in following calculations, considering computational efficiency.

Taking convergence tolerance as the criterion of aerostatic instability not only intuitively reflect the convergence of the wind loads but also indirectly the convergence of the structural deformation. However, the onset wind velocity of aerostatic instability is related to the Euclidean norm convergence tolerance due to the introduction of a artificial convergence tolerance. Excessive convergence tolerance may lead to overestimation of the

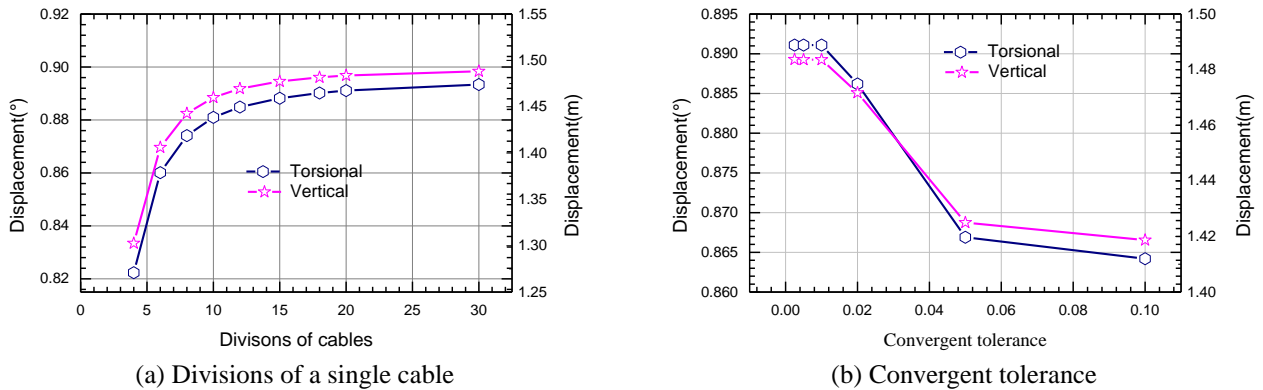


Fig. 12 Variation of displacements of bridge deck at the center node of the left main span

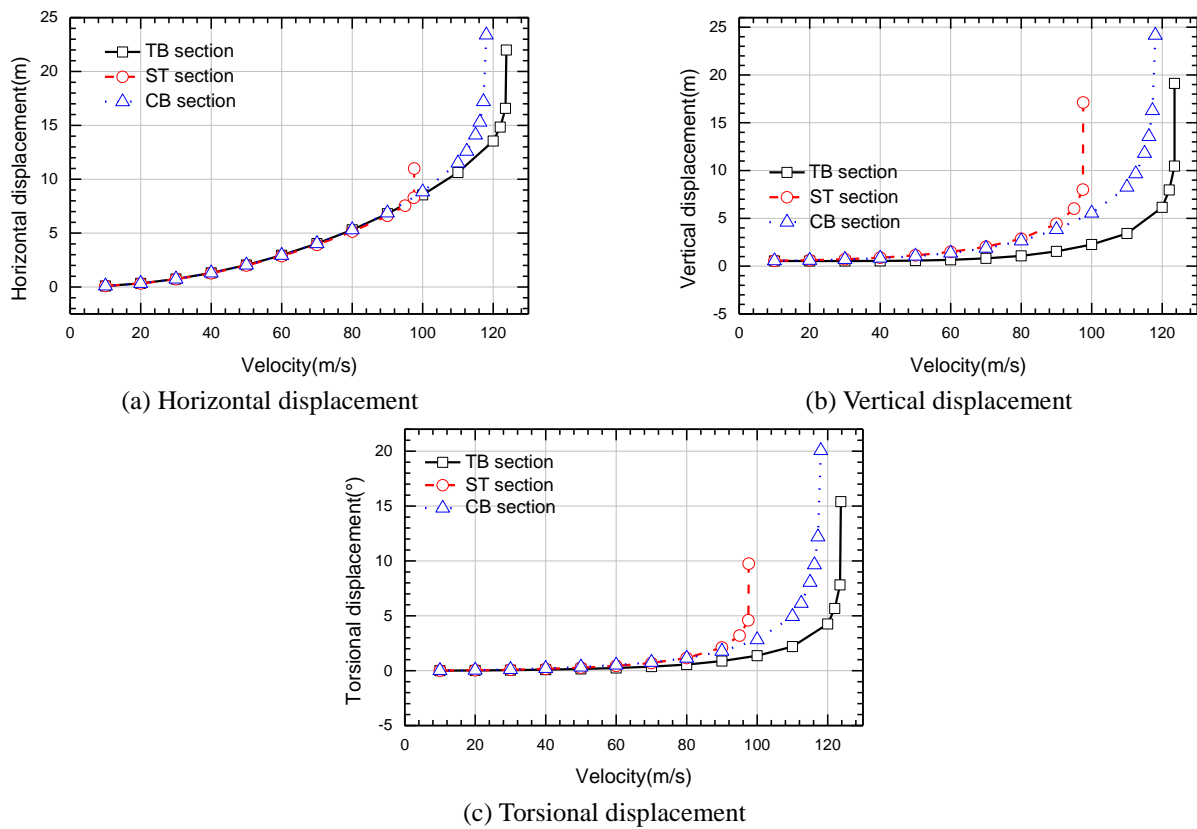


Fig. 13 Comparison of responses at the center node of the left main span between different bridge decks at initial attack angle of  $+3^\circ$

aerostatic stability of the bridges. Variation of vertical and torsional displacements with the convergence tolerances at 110 m/s at initial attack angle of  $0^\circ$  (twin-box section), are shown in Fig. 12(b). It is shown that both torsional and vertical displacements do not vary significantly with the convergence tolerances when the convergence tolerances are less than or equal to 0.005. Thus, the convergence tolerance is here set to 0.0025 in following calculations.

As indicated in section 2.2.1, the drag, lift, and pitching moment of the bridge decks are measured based on sectional model with scale ratio of 1/70 or 1/80. In order to keep in line with the static aerodynamic coefficients of the

bridge decks above, the geometrical scale ratio of the cables was taken as the same value, and then an intermediate value of 1/75 is set here. Thus, the corresponding Reynolds number for a cable with diameter of the real bridge ranging from 0.083 m to 0.124 m, lies between  $7.48 \times 10^2$  and  $1.68 \times 10^4$ , when the tested wind velocities range from 10 m/s to 150 m/s. It should be noted that the drag coefficient of a cable will pass from the sub-critical range to the super-critical range in that wind velocity range, which are neglected in this research. Besides, the aspect ratios ( $L/D$ ) of the cables are far larger than 2000. Where  $L$  denotes the length of a cable, and  $D$  denotes the diameter of a cable.

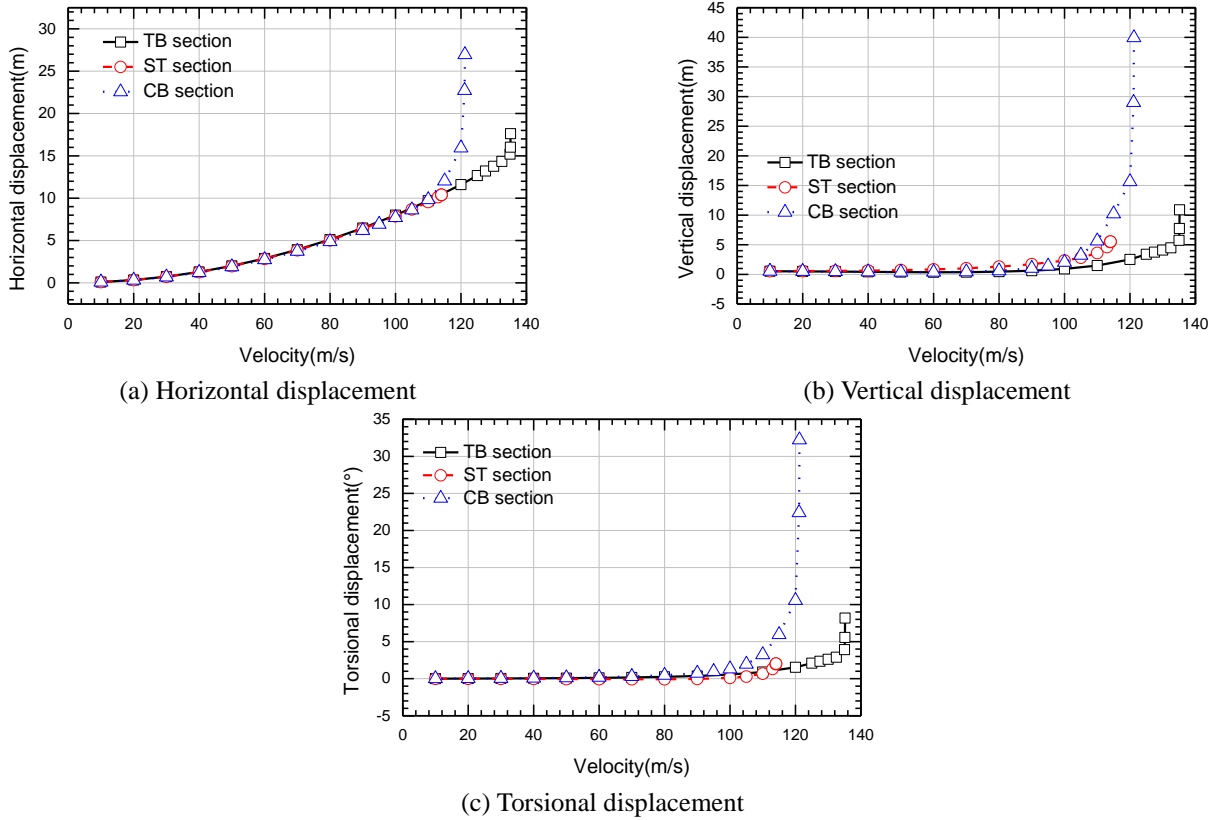


Fig. 14 Comparison of responses at the center node of the left main span between different bridge decks at initial attack angle of 0°

According to Daugherty *et al.* (2011), the drag coefficient of a infinite circular cylinder and a circular cylinder with aspect ratio of 115 approximately ranges from 1.1 to 1.2. Therefore, the drag coefficient of cables is set to 1.20 in the research, ignoring variation of the drag coefficient of a cable with wind velocity in the instability process, for convenience. In addition, the shielding effects of the cable plane in leeward side are just neglected due to complexity of aerodynamic interference between multi-cylinders.

## 4. Results and discussion

### 4.1 Aerostatic stability

The comparison of horizontal, vertical, and torsional displacements at the center node of the left main span are depicted, at initial attack angle of +3°, 0°, and -3°, in Figs. 13-15 respectively. There exhibits distinct torsional, vertical, and lateral three-way coupling in the process of aerostatic instability at all initial attack angles. The directions of vertical and torsional responses for all bridge decks at initial attack angles of +3° and 0° are opposite to those at initial attack angle of -3°.

Table 3 lists the onset wind velocity of the aerostatic torsional divergence of the twin-box, the stiffening truss, and the closed-box section at initial attack angle of +3°, 0°, and -3°. The onset velocities of the stiffening truss section are the lowest, those of the closed-box section are the

second lowest, and those of the twin-box section are the highest at initial attack angles of +3° and 0°. In addition, it is also interesting to find that the most unfavorable initial attack angle is +3° for each bridge deck, and the onset wind velocities at initial attack angle of +3° are much lower than those at initial attack angle of -3°.

### 4.2 Flutter stability

Flutter derivatives related to lateral motions are determined based on the quasi-steady theory (Ding *et al.* 2002), and can be expressed as follows

$$P_1^* = -\frac{1}{K} C_D \quad (3a)$$

$$P_2^* = \frac{1}{2K} (dC_D/d\alpha) \quad (3b)$$

$$P_3^* = \frac{1}{2K^2} C_D' \quad (3c)$$

$$P_5^* = \frac{1}{2K} (dC_D/d\alpha) \quad (3d)$$

$$H_5^* = \frac{1}{2K} C_L \quad (3e)$$

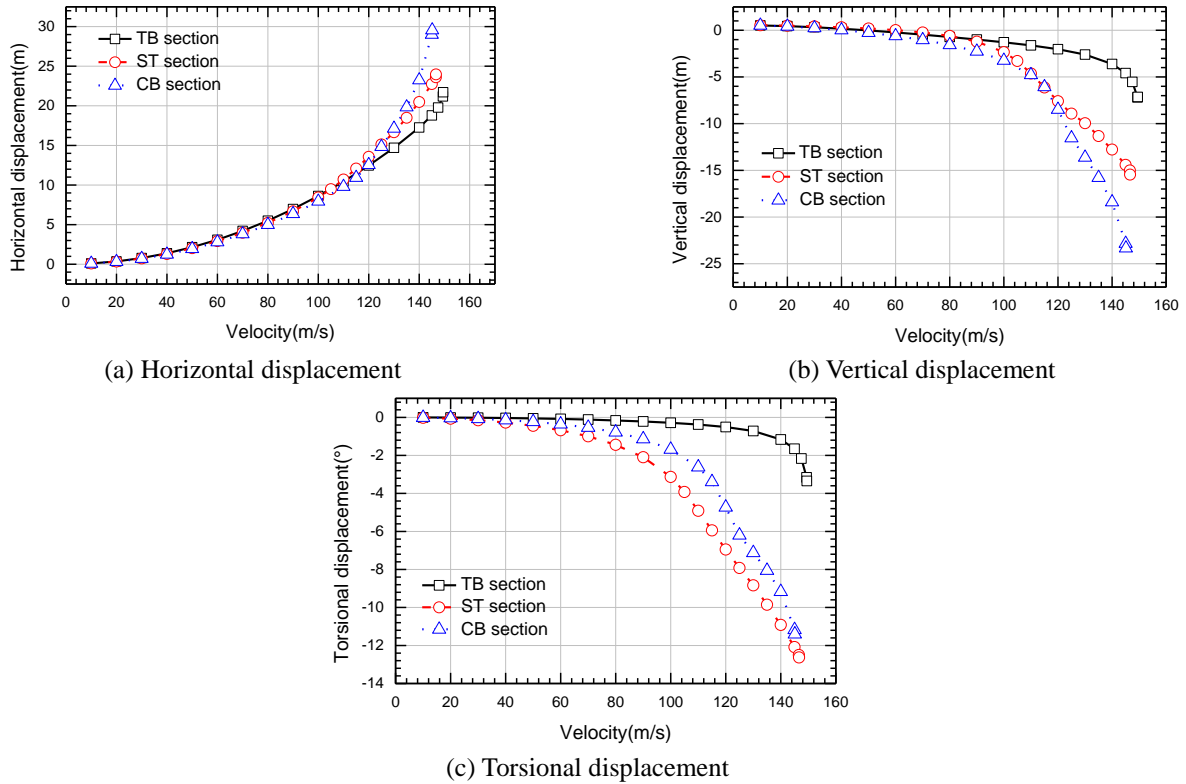


Fig. 15 Comparison of responses at the center node of the left main span between different bridge decks at initial attack angle of  $-3^\circ$

Table 3 Onset wind velocity of aerostatic torsional divergence (Unit: m/s)

Initial attack	+3°	0°	-3°
TB section	123.8	135.2	149.5
ST section	97.6	114.0	146.7
CB section	118.1	120.2	145.1

Table 4 Main modes of the bridge

Mode no.	Frequency (Hz)	Mode shape
1	0.0620	A-L-1
2	0.0673	S-L-1
3	0.1009	A-V-1
4	0.1325	S-V-1
5	0.1384	A-V-2
6	0.1484	A-V-3
7	0.1563	S-L-2
8	0.1646	A-L-2
10	0.2130	S-V-2
13	0.2416	A-V-4
14	0.2562	S-V-3
15	0.2851	A-V-5
18	0.3008	S-V-4
19	0.3087	A-V-6
20	0.3157	S-V-5
21	0.3210	S-V-6
27	0.3764	A-T-1
28	0.3876	S-T-1
40	0.5024	A-T-2
41	0.5077	S-T-2

$$A_5^* = -\frac{1}{K} C_M \quad (3f)$$

$$P_4^* = P_6^* = A_6^* = H_6^* = 0 \quad (3g)$$

where,  $dC_D/d\alpha$  denotes the first derivative of the  $C_D$  versus  $\alpha$ . Thus, all flutter derivatives were determined based on the flutter derivatives, as shown in Figs. 9-11, and static aerodynamic coefficients, as shown in Fig. 7.

The method of three-dimensional (3D) multimode flutter analysis proposed by Ding *et al.* (2002) were conducted to obtain the onset velocities of flutter. The structural damping ratio for each natural mode is assumed to 0.003. The first 50 natural modes are computed by the Lanczos method, and the major modes of the bridge are listed in

\* S: Symmetric; A: Anti-symmetric; V: Vertical; L: Lateral; T: Torsional

Table 5 Comparison of flutter onset velocities (Unit: m/s)

Initial attack angle (°)	+3	0	-3
TB section	174.0	>200	>200
ST section	126.5	146.1	157.4
CB section	70.8	112.4	>200

Table 4 the lists 1<sup>st</sup>-order symmetrical vertical and 1<sup>st</sup>-order symmetrical torsional mode diagrams are shown in Table 5. The Sturm check on the first 50 modes was conducted to prevent the missing of modes, and no mode is found missing. Then a comparison of flutter onset velocities at initial attack angle of  $-3^\circ$ ,  $0^\circ$ , and  $+3^\circ$  is shown in Table 5.

The onset velocities of all bridge decks at initial attack angle of  $+3^\circ$  are lower than those at other initial attack angles. The onset velocities of flutter are highest for the twin-box section, followed by the stiffening truss section, and finally the closed-box section, indicating that the flutter stability of twin-box section is much better than that of the stiffening truss section and closed-box section.

#### 4.3 Competitive relationships

In order to quantitatively evaluate the competitive relationships between aerostatic stability and flutter stability, the dimensionless coefficient - stability ratio is defined as follows

$$\text{Stability ratio} = \frac{\text{Critical wind velocity of aerostatic instability}}{\text{Critical wind velocity of flutter instability}} \quad (3)$$

The stability ratios at initial attack angle of  $-3^\circ$ ,  $0^\circ$ , and  $+3^\circ$  are listed in Table 6. Stability ratios of the twin-box section are far below 1.0 at all initial attack angles, indicating that wind-resistance design for the bridge with twin-box section totally depends on the control of aerostatic instability. Stability ratios of the stiffening truss section are far below 1.0 at initial attack angle of  $0^\circ$  and  $+3^\circ$ , and close to 1.0 at initial attack angle of  $-3^\circ$ . Stability ratios of the closed-box section are much greater than 1.0 at initial attack angle of  $+3^\circ$ , while far below 1.0 at initial attack angle of  $-3^\circ$ , close to 1.0 at initial attack angle of  $0^\circ$ . This shows that competitive relationships between aerostatic and flutter instability for the closed-box section vary dramatically with initial attack angle to a great extent.

The onset wind velocities of control design are obtained from the lower value between the onset velocities of aerostatic instability and flutter for each bridge deck. Fig. 16 shows the variation in the onset wind velocity with initial attack angle. The onset wind velocities decrease as the initial attack angle increase, and the initial attack angle of  $+3^\circ$  is the most unfavorable. The onset wind velocities of control design of the twin-box section are found to be higher than those of the other sections.

In short, aerostatic instability occur earlier than flutter both for the twin-box section and stiffening truss section. There are dramatic competitive relationships between aerostatic instability and flutter for the closed-box section.

Table 6 Comparison of stability ratios

Initial attack angle/(°)	+3	0	-3
TB section	0.711	<0.676	<0.748
ST section	0.772	0.780	0.932
CB section	1.668	1.069	<0.726

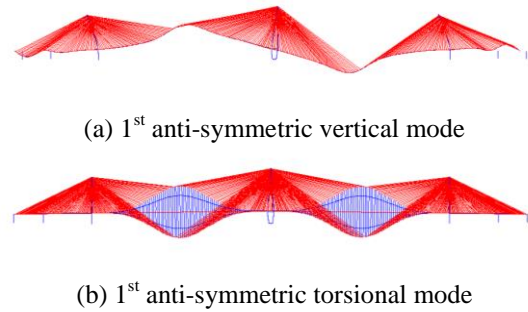


Fig. 16 Shape diagram

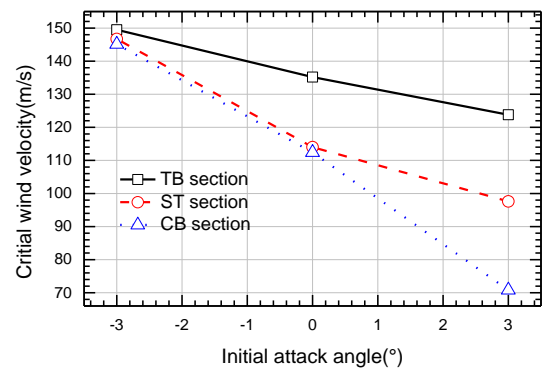


Fig. 17 Variation in the onset wind velocity of control design with the initial attack angle

Flutter occur before aerostatic instability at initial attack angle of  $+3^\circ$ , while aerostatic instability occur before flutter at initial attack angle of  $-3^\circ$  and  $0^\circ$ .

#### 5. Mechanism of aerostatic torsional divergence

Comparisons of tensile stresses for the cable located at the center node of the left main span between different bridge decks at initial attack angle of  $+3^\circ$ ,  $0^\circ$ , and  $-3^\circ$ , are shown in Figs. 17 and 18 respectively. Combined with responses of the bridge decks at the center node of the left main span in Section 3, mechanism of aerostatic torsional divergence can be analyzed as follows.

For initial attack angle of  $+3^\circ$  and  $0^\circ$ . At the initial stage, torsional motions are dominant, resulting in the downward movement of the downstream side of the bridge deck, leading to the stretching of the cables at that side, and the downstream cable tensions increase with wind velocities until the upward vertical movements are dominant. Then the downstream cables are also relaxed and sag effects are

more obvious, resulting in decrease in cable tensions and structural stiffness as the wind velocities increase. The deformation of the bridge decks increases under the action of the pitching moment, which lead to the structural instability, and the cycle continues.

For initial attack angle of  $-3^\circ$ , the bridge deck always moves downwards, stretching the cables, and both the upstream and downstream cable tensions for each bridge deck increase as wind velocities increase until the structure become unstable.

The mechanism underlying aerostatic torsional divergence at positive initial attack angles is found to be markedly different from that at negative initial attack angles. The bridge deck moves upwards at initial attack angle of  $+3^\circ$  as wind velocity increases, resulting in the relaxation of the cables, thus destroying the stable triangular relationships between the cable planes at each end of the bridge deck and the bridge deck, and structural stiffness decreases sharply, leading to aerostatic torsional divergence; However, the bridge deck at initial attack angle of  $-3^\circ$  generally do not move upwards, and cable tension increases while the bridge deck moves downwards.

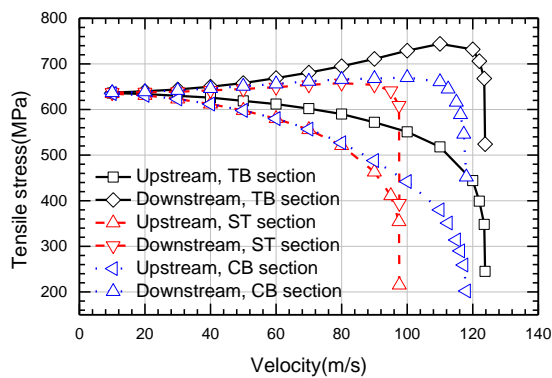


Fig. 18 Comparison of tensile stresses for the cable located at the center node of the left main span between different bridge decks at initial attack angle of  $+3^\circ$

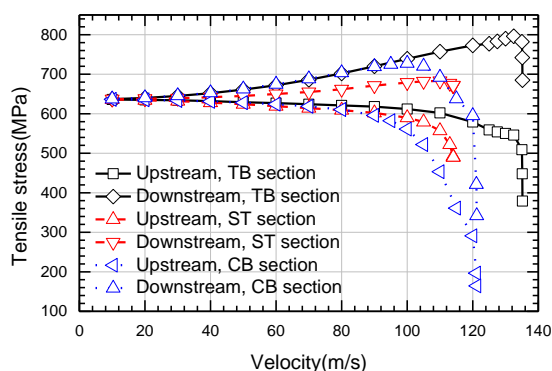


Fig. 19 Comparison of tensile stresses for the cable located at the center node of the left main span between different bridge decks at initial attack angle of  $0^\circ$

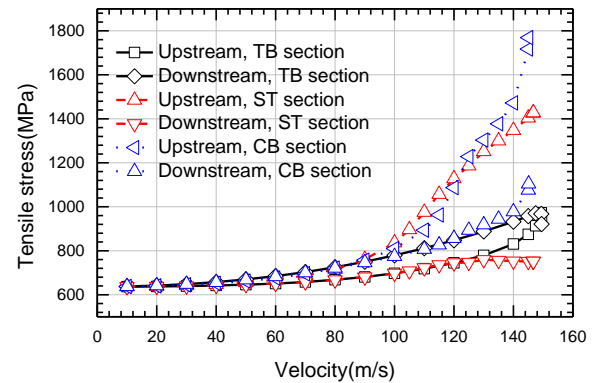


Fig. 20 Comparison of tensile stresses for the cable located at the center node of the left main span between different bridge decks at initial attack angle of  $-3^\circ$

Then the stable triangular relationships between the cable planes at each end of the bridge deck and the bridge deck are not destroyed, so the structural stiffness decreases slowly and the onset wind velocity is higher than that at initial attack angle of  $+3^\circ$ . It is found the onset wind velocity of different bridge decks to be very close at initial attack angle of  $-3^\circ$ , which further indicates that the stable structure, comprised of the cable planes, the tower, and the bridge deck greatly improves the aerostatic stability of the bridge, while the aerodynamic effects associated with the aerodynamic configurations of the bridge decks had little effects on the aerostatic stability at initial attack angle of  $-3^\circ$ .

Comparisons of the torsional displacements between different bridge decks in the critical state at initial attack angles of  $+3^\circ$ ,  $0^\circ$ , and  $-3^\circ$ , are shown in Figs. 21-23, respectively. Results show that the instability patterns of stiffening truss section and closed-box section are basically symmetrical and the maximum displacement is located at the center of the main span. Whereas the instability pattern of the twin-box section is found to be markedly different from that of the other bridge decks at initial attack angle of  $-3^\circ$ . Furthermore, instability patterns of the closed-box section are not symmetric at initial attack angle of  $+3^\circ$  and  $0^\circ$ , which is obviously different from other bridge decks. The reason for this is expressed as follows.

As shown in Table 4, the natural frequencies of the 1<sup>st</sup> asymmetric modes are very close to those of the 1<sup>st</sup> symmetric modes, especially for the torsional modes, with error of less than 1%, indicating that energy for anti-symmetric deformation excitation are close to that for symmetric deformation excitation. Therefore, the instability pattern is dominated by both the 1<sup>st</sup>-order symmetric and anti-symmetric modes, depending on the initial attack angles and the static aerodynamic coefficients, that is, aerodynamic configurations of the bridge decks. Thus, it is natural that the torsional displacement is not symmetric although the structure is symmetric for the closed-box section, which is different from the other bridge decks.

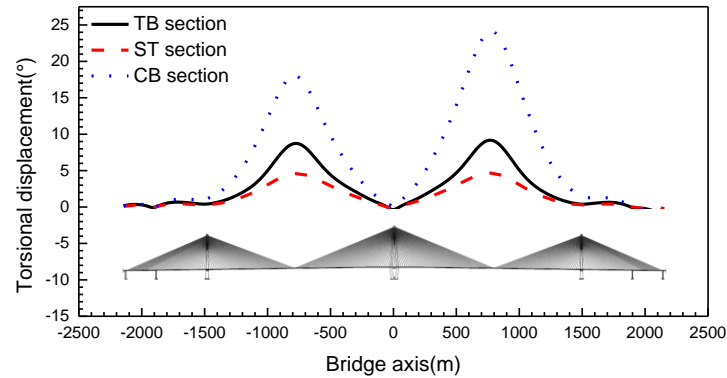


Fig. 21 Comparison of torsional displacements in the critical state at initial attack angle of  $+3^\circ$

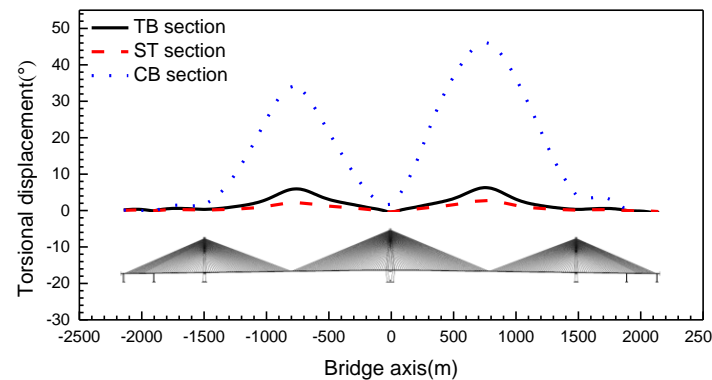


Fig. 22 Comparison of torsional displacements in the onset state at initial attack angle of  $0^\circ$

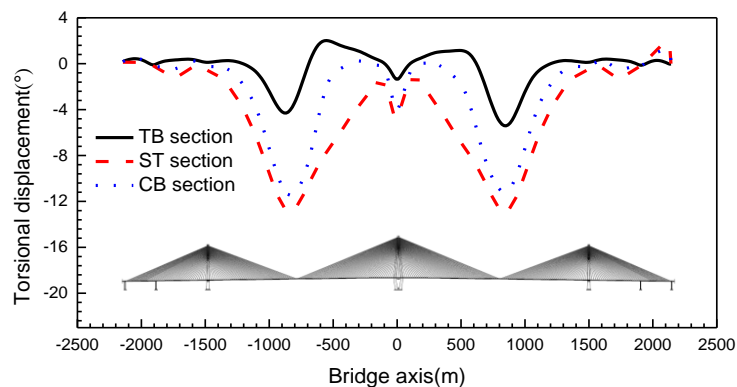


Fig. 23 Comparison of torsional displacements in the critical state at initial attack angle of  $-3^\circ$

## 6. Conclusions

Based on a long-span cable-stayed bridge with double main spans of 1500 m, combined wind tunnel tests with numerical calculations comprised of three-dimensional (3D) multimode flutter analysis and nonlinear aerostatic analysis, typical bridge decks, involving twin-box, stiffening truss, and closed-box section, are chosen to investigate effects of aerodynamic configurations on the aerostatic stability and flutter stability of the bridge, and the competitive relationships between them are also investigated at initial attack angles of  $-3^\circ$ ,  $0^\circ$ , and  $+3^\circ$ . Then mechanisms of

aerostatic torsional divergence are revealed by tracking the cable tensions synchronous with deformation of the bridge decks in the instability process. The main conclusions are summarized as follows:

The onset velocities of aerostatic instability for different bridge decks are markedly different, and vary with the initial attack angle. The aerostatic stability of the twin-box section is the best, and that of the stiffening truss section is the worst. Moreover, the most unfavorable initial attack angles is  $+3^\circ$  for all bridge decks.

The flutter stability of the twin-box section is the best at initial attack angle of  $-3^\circ$ ,  $0^\circ$ , and  $+3^\circ$ , while that of the closed-box section is the worst. The flutter stability of the

twin-box section is substantially better than that of the stiffening truss and closed-box section.

Aerostatic instability occur earlier than flutter for the twin-box section and stiffening truss section. There are clear competitive relationships between aerostatic instability and flutter for the closed-box section. Flutter occur before aerostatic instability at initial attack angle of  $+3^\circ$  and  $0^\circ$ , while aerostatic instability occur before flutter at initial attack angle of  $-3^\circ$ .

The mechanism underlying aerostatic torsional divergence at positive initial attack angles is found to be markedly different from that at negative initial attack angles. The onset wind velocities of aerostatic instability at initial attack angle of  $+3^\circ$  are much lower than those at initial attack angle of  $-3^\circ$  for all the bridge decks due to the stable triangular relationships between the cable planes at each end of the bridge deck and the bridge deck. And the onset wind velocities of these bridge decks are very similar at initial attack angle of  $-3^\circ$ . This indicates that a stable triangular structure made up of the cable planes, the tower, and the bridge deck greatly improves the aerostatic stability of the structure, while the aerodynamic effects associated with the aerodynamic configurations of the bridge decks have little effects on the aerostatic stability at initial attack angle of  $-3^\circ$ . In addition, instability patterns of the bridge depend on both the initial attack angles and aerodynamic configurations of the bridge decks.

In this way, aerodynamic configurations have visible effects on the aerostatic stability and flutter stability of the bridge, as well as the competitive relationships between them, and they are shown to vary with the initial attack angle. This study is helpful in determining bridge decks for super long-span bridges in future.

## Acknowledgments

The research described in this paper was financially supported by the Natural Science Foundation.

## References

- Argentini, T., Diana, G., Rocchi, D. and Somaschini, C. (2016), "A case-study of double multi-modal bridge flutter: experimental result and numerical analysis", *J. Wind Eng. Ind. Aerod.*, **151**, 25-36.
- Boonyapinyo, V., Lauhatanon, Y. and Lukkunaprasit, P. (2006), "Nonlinear aerostatic stability analysis of suspension bridges", *Eng. Struct.*, **28**(5), 793-803.
- Boonyapinyo, V., Yamada, H. and Miyata, T. (1994), "Wind-induced nonlinear lateral-torsional buckling of cable-stayed bridges", *J. Struct. Eng.*, **120**(2), 486-506.
- Chen, J. (2000), "Study on nonlinear aerostatic stability of cable-supported bridges", Ph.D. Dissertation, Tongji University, Shanghai, China. (in Chinese)
- Chen, J., Xiao, R.C. and Xiang H.F. (2001), "Study on parameters of aerostatic stability of long-span cable-stayed bridges", *China Civil Eng. J.*, **34**(2), 55-61. (in Chinese)
- Cheng, J., Jiang, J.J., Xiao, R.C. and Xiang, H.F. (2002), "Nonlinear aerostatic stability analysis of jiang yin suspension bridge", *Eng. Struct.*, **24**(6), 773-781.
- Cheng, J., Xiao, R.C., Xiang, H.F. and Jiang, J.J. (2003), "Nasab: a finite element software for the nonlinear aerostatic stability analysis of cable-supported bridges", *Adv. Eng. Softw.*, **34**(5), 287-296.
- Daugherty, R.L., Franzini, J.B. and Finnemore, E.J. (2011), *Fluid Mechanics with Engineering Applications*, (9th Ed.), New York, NY, USA.
- Diana, G., Falco, M., Bruni, S., Cigada, A., Larose, G.L., Darnsgaard, A., et al. (1995), "Comparisons between wind tunnel tests on a full aeroelastic model of the proposed bridge over stretto di messina and numerical results", *J. Wind Eng. Ind. Aerod.*, **54-55**(94), 101-113.
- Diana, G., Resta, F., Zasso, A., Belloli, M. and Rocchi, D. (2004), "Forced motion and free motion aeroelastic tests on a new concept dynamometric section model of the Messina suspension bridge", *J. Wind Eng. Ind. Aerod.*, **92**, 441-462.
- Ding, Q.S., Chen, A.R. and Xiang, H.F. (2002), "Coupled flutter analysis of long-span bridges by multimode and full-order approaches", *J. Wind Eng. Ind. Aerod.*, **90**(12), 1981-1993.
- Ge, Y.J. (2011), "Wind-resistance of Long Span Suspension Bridges", *China Communications Press*, Beijing, China. (in Chinese)
- Ge, Y.J. and Xiang, H.F. (2009), "Bluff body aerodynamics application in challenging bridge span length", *Proceedings of the BBAA VI International Colloquium on: Bluff Bodies Aerodynamics & Applications*, Milano, Italy, July, 20-24.
- Hirai, A., Okauchi, I., Ito, M. and Miyata, T. (1967), "Studies on the onset wind velocity for suspension bridges", *Proceedings of the International Research Seminar on Wind Effects on Buildings and Structure*, Ontario: University of Toronto Press.
- Kavrov, I. and Morgenthal, G. (2017), "A comparative assessment of aerodynamic models for buffeting and flutter of long-span bridges", *Engineering*, **3**(6), 823-838.
- Kitagawa, M. (2004), "Technology of the akashi kaikyo bridge", *Struct. Control Health Monit.*, **11**(2), 75-90.
- Kusano, I., Baldomir, A., Jurado, J.A. and Hernández, S. (2014), "Reliability based design optimization of long-span bridges considering flutter", *J. Wind Eng. Ind. Aerod.*, **135**, 149-162.
- Laima, S. and Li, H. (2015), "Effects of gap width on flow motions around twin-box girders and vortex-induced vibrations", *J. Wind Eng. Ind. Aerod.*, **139**, 37-49.
- Larose, G.L. and D'auiteuil, A. (2006), "One the Reynolds number sensitivity of the aerodynamics of bluff bodies with sharp edges", *J. Wind Eng. Ind. Aerod.*, **94**(5), 365-376.
- Lee, S., Kwon, S.D. and Yoon, J. (2014), "Reynolds number sensitivity to aerodynamic forces of twin box bridge girder", *J. Wind Eng. Ind. Aerod.*, **127**(127), 59-68.
- Li, H., Laima, S. and Jing, H. (2014), "Reynolds number effects on aerodynamic characteristics and vortex-induced vibration of a twin-box girder", *J. Fluid. Struct.*, **50**, 358-375.
- Li, J.W., Fang, C., Hou, L.M. and Wang, J. (2014), "Sensitivity analysis for aerostatic stability parameter of a long-span bridge", *J. Vib. Shock*, **33**(4), 124-130. (in Chinese)
- Mannini, C. and Bartoli, G. (2015), "Aerodynamic uncertainty propagation in bridge flutter analysis", *Struct. Saf.*, **52**, 29-39.
- Matsuda, K., Cooper, K.R., Tanaka, H., Tokushige, M. and Iwaski, T. (2001), "An investigation of Reynolds number effects on the steady and unsteady aerodynamic forces on a 1:10 scale bridge deck section model", *J. Wind Eng. Ind. Aerod.*, **89**(7), 619-632.
- Miranda, S.D., Patruno, L., Ricci, M. and Ubertini, F. (2015), "Numerical study of a twin box bridge deck with increasing gap ratio by using RANS and LES approaches", *Eng. Struct.*, **99**, 546-558.

- Scanlan, R.H. (1978), "The action of flexible bridges under wind, I: flutter theory", *J. Sound Vib.*, **60**(2), 187-199.
- Scanlan, R.H. (1993), "Problematic in formulation of wind-force model for bridge decks", *J. Struct. Eng. - ASCE*, **119**, 1433-1446.
- Schewe, G. (2001), "Reynolds-number effects in flow around more-or-less bluff bodies", *J. Wind Eng. Ind. Aerod.*, **89**(14), 1267-1289.
- Schewe, G. and Larsen, A. (1998), "Reynolds number effects in the flow around a bluff bridge deck cross section", *J. Wind Eng. Ind. Aerod.*, **74-76**(2), 829-838.
- Trein, C.A., Shirato, H. and Matsumoto, M. (2015), "On the effects of the gap on the unsteady pressure characteristics of two-box bridge girders", *Eng. Struct.*, **82**, 121-133.
- Yang, Y., Zhou, R., Ge, Y., Mohotti, D. and Mendis, P. (2015), "Aerodynamic instability performance of twin box girders for long-span bridges", *J. Wind Eng. Ind. Aerod.*, **145**, 196-208.
- Yang, Y.X., Ge, Y.J. and Xiang, H.F. (2007), "Investigation on flutter mechanism of long-span bridges with 2d-3DOF method", *Wind Struct.*, **10**(5), 421-435.
- Zhang, X.J. (2007), "Influence of some factors on the aerodynamic stability of long-span suspension bridges", *J. Zhejiang Univ. Technol.*, **95**(3), 149-164. (in Chinese)
- Zhang, Z.T., Ge, Y.J. and Yang, Y.X. (2013), "Torsional stiffness degradation and aerostatic divergence of suspension bridge decks", *J. Fluid. Struct.*, **40**(7), 269-283.
- Zhu, L.D., Xiang, H.F. and Xu, Y.L. (2000), "Triple-girder model for modal analysis of cable-stayed bridges with warping effect", *Eng. Struct.*, **22**(10), 1313-1323.

AD